

Proceeding Paper

Electronic Structures of Eu-Doped FAPbI₃ Perovskite Crystals Studied by First-Principles Calculation †

Atsushi Suzuki *  and Takeo Oku 

Department of Materials Science, The University of Shiga Prefecture, 2500 Hassaka, Hikone 522-8533, Japan; oku@mat.usp.ac.jp

* Correspondence: suzuki@mat.usp.ac.jp; Tel.: +81-749-28-8369

† Presented at the 3rd International Online Conference on Crystals, 15–30 January 2022; Available online: https://iocc_2022.sciforum.net/.

Abstract: The effects of mixed-valence states on electronic structures of europium (Eu)-incorporated CH(NH₂)₂PbI₃ (FAPbI₃) and CH₃NH₃PbI₃ (MAPbI₃) perovskite crystals were investigated by first-principles calculation. Partial replacements of europium ions into the perovskite crystals influenced the electronic structures. In the case of the FAPb(Eu⁺³)I₃ crystal, there was wide distribution of the 5p orbital of iodine near the valence band, and of the 3d orbital of the Eu³⁺ ion near the conductive band. Incorporation of Eu²⁺ ions into the perovskite crystal provided low energy levels at the VB, with an increase in the bandgap and a decrease in m_h^*/m_e . This behaviour suggests improvement of carrier mobility related to short-circuit current and conversion efficiency, as compared with the incorporation of Eu³⁺ ions into the perovskite crystal. The partial substitution of europium ions at the position of lead ions as the B-site in the perovskite crystal caused the electron correlation based on the charge transfer between the 5p orbital of iodine and the 3d orbital of Eu ions, and narrowed the band dispersion with a decrease in the effective mass ratio, which was expected to improve the carrier mobility related to the short-circuit current density and the conversion efficiency.

Keywords: perovskite crystal; first-principles calculation; band structure; NMR



Citation: Suzuki, A.; Oku, T.

Electronic Structures of Eu-Doped FAPbI₃ Perovskite Crystals Studied by First-Principles Calculation. *Chem. Proc.* **2022**, *9*, 12. https://doi.org/10.3390/IOCC_2022-12178

Academic Editor: Arcady Zhukov

Published: 9 February 2022

Publisher's Note: MDPI stays neutral with regard to jurisdictional claims in published maps and institutional affiliations.



Copyright: © 2022 by the authors. Licensee MDPI, Basel, Switzerland. This article is an open access article distributed under the terms and conditions of the Creative Commons Attribution (CC BY) license (<https://creativecommons.org/licenses/by/4.0/>).

1. Introduction

Perovskite solar cells have great advantages for developing photovoltaic applications using perovskite crystals with variable elemental composition and crystal structure [1–3]. The perovskite solar cells have high performance in terms of photovoltaic properties. A wide-bandgap perovskite tandem solar cell has been developed for practical use of photovoltaic devices [4,5]. The photovoltaic properties are influenced by the chemical elements and crystalline structure in the active layer [6,7]. The photovoltaic performance is based on optimisation with tuning of the band structure and the effective mass related to carrier mobility. For example, incorporation of alkali metals [8–10], organic cations [11,12], transition metals [13–20], tin [21,22], and halogen ions [23,24] improved the photovoltaic performance. The decomposition was suppressed by partial substitution of formamidinium (FA) [25], guanidinium (GA), ethylammonium (EA), and alkali metal ions instead of methyl ammonium (MA) at the A-sites, and transition metals (e.g., copper [18,19], cobalt [26], and nickel) were incorporated with lead (Pb) ions at the B-sites in the CH₃NH₃PbX₃ (MAPbX₃) perovskite crystal, where X represents the halogen ions. The surface modifications promoted the carrier diffusion by suppressing the deterioration.

The photovoltaic performances were associated with the electronic structure [27,28]. The tolerance factor with variable effective ionic radii was used for predicting the thermodynamic stability of the crystal as a cubic crystal system [29]. Transition-metal-incorporated perovskite crystal had a high potential for improved photovoltaic properties [30,31]. Recently, the photovoltaic properties of lanthanide perovskite compounds were characterised

by experimental methods using first-principle calculation [32–35]. Rare-earth-based compounds have unique physical phenomena, such as heavy-electron behaviour [36,37]. The photovoltaic performance, electronic structure, and partial density of state were studied by first-principle calculations using density functional theory (DFT) [38–41]. Partial replacement of europium ions at the B site in the perovskite crystal prevented the decomposition, improving the stability of the performance.

The purpose of the present study was to focus on improvement of the photovoltaic properties by investigating the effects of europium in the FAPbI₃ perovskite crystal. The electronic structure of the Eu-incorporated FAPbI₃ perovskite crystal was predicted by first-principles calculations. The electronic structures, electron density distribution, band structure, partial density of state (pDOS), chemical shifts of ¹²⁷I-NMR, electronic field gradient (EFG), and asymmetry parameter (η) were considered in the Eu-incorporated FAPbI₃ or MAPbI₃ perovskite crystals. The photovoltaic mechanism was discussed with reference to the electronic structure.

2. Calculation

The electronic structures of the perovskite crystals were single-point-calculated with crystallographic structural data obtained from X-ray diffraction patterns. The ab initio quantum calculations were performed using the Vanderbilt ultrasoft pseudopotentials, scalar relativistic generalised gradient approximations and Perdew–Burke–Ernzerhof (GGA-PBE) exchange–correlation functional, and density functional theory (DFT + U, U = 6.0 eV) (Quantum Espresso software). The basis functions were used properly according to the cases of itinerant and localised electron systems. Plane-wave basis cutoffs for the wave functions and charge density were set at 25 and 225 Rydberg (Ry), respectively. The perovskite crystals were constructed with experimental lattice constants ($a = 6.362 \text{ \AA}$) and a crystal system (cubic $Pm3m$) [41,42]. A uniform k -point grid ($4 \times 4 \times 4$) in the Brillouin zone was used to calculate the electronic structure and partial density of state. The Eu-incorporated FAPbI₃ perovskite cubic crystal models were constructed with the supercells ($2 \times 2 \times 2$) as the initial unit cells, and were used for the band calculation. The band structures and effective mass were analysed for the Brillouin zone of the perovskite crystal along the direction of the wave vector.

The paths for the FAPbI₃ perovskite crystals were set as follows: $\Gamma (0, 0, 0) \rightarrow X (0, \frac{1}{2}, 0) \rightarrow M (1/2, 1/2, 0) \rightarrow \Gamma \rightarrow R (1/2, 1/2, 1/2) \rightarrow X, M \rightarrow R$. The Pb cation was set at the position of $\Gamma (0, 0, 0)$. The FA cation was set in the centre position of the unit cell ($1 \times 1 \times 1$). The paths for the FAPb(Eu)I₃ perovskite crystals were set as follows: $\Gamma (0, 0, 0) \rightarrow X (1/2, 0, 1/2) \rightarrow W (1/2, 1/4, 3/4) \rightarrow K (3/8, 3/8, 3/4) \rightarrow \Gamma \rightarrow L (1/2, 1/2, 1/2) \rightarrow U (5/8, 1/4, 5/8) \rightarrow W (1/2, 1/4, 3/4) \rightarrow L \rightarrow K \mid U \rightarrow X$. For minor partial replacement, the Eu cation was replaced with a Pb cation in the centre position of the supercell ($2 \times 2 \times 2$). The density of states (DOS) and partial density of states (pDOS) were calculated to make clear the energy levels for each orbital near the valence band (VB) and conduction band (CB). The chemical shifts of ¹²⁷I-NMR, ¹⁵⁷Eu-NMR, electronic field gradient (EFG), and the asymmetry parameter (η) of the Eu-doped MAPbI₃ crystal were calculated via hybrid DFT using unrestricted B3LYP (UB3LYP) and GIAO, with SSDall as the basis set (Gaussian 09).

3. Results and Discussion

The band structure, partial density of state, and electronic density distribution in the FAPb(Eu³⁺)I₃ perovskite crystal were calculated by first-principles calculation. The band structure, partial density of state (pDOS), and electronic density distribution in the FAPb(Eu³⁺)I₃ perovskite crystal are shown in Figure 1a. The energy levels at the valence band and conduction band, bandgap, and the effective mass ratio of electrons and holes in the electron structure were calculated. The direct bandgap was found to be 1.45 eV. The band-dispersion curvature at the wave vector near path: $\Gamma (0, 0, 0) \rightarrow R (1/2, 1/2, 1/2)$ had an effective mass ratio of electrons and holes of 0.04 and 0.07, indicating the minimum value and anisotropy carrier behaviour depending on the crystal orientation.

This result indicates that it is easy for carriers to diffuse in the crystal, improving the carrier mobility, short-circuit current density, and conversion efficiency. The partial density of state and enlarged view of 3p, 3d, and 4f of Eu^{3+} in the $\text{FAPb}(\text{Eu}^{3+})\text{I}_3$ perovskite crystal were considered. The 5p orbital of iodine and the 3d and p orbitals of Eu^{3+} were widely distributed near the valence band state. Near the conduction band, the 6p orbital of Pb and the 3d and 4f orbitals of Eu^{3+} were widely distributed. The itinerant behaviour indicates a different tendency from the localised system of the FAEuI_3 perovskite crystal [39].

In the case of the $\text{FAPb}(\text{Eu}^{2+})\text{I}_3$ perovskite crystal, the band structure and pDOS were considered, as shown in Figure 1b. The band structure had a direct bandgap of E_g of 1.53 eV near the wave vector at Γ (0, 0, 0). The band-dispersion curvature near at Γ (0, 0, 0) had an effective mass of electrons and holes of 0.03 and 0.01, respectively. The itinerant characteristics indicate the light electronic system. The carriers could easily diffuse with the increase in mobility in the $\text{FAPb}(\text{Eu}^{2+})\text{I}_3$ perovskite crystal, as compared with those in the $\text{FAPb}(\text{Eu}^{3+})\text{I}_3$ perovskite crystal. The partial density of state and the enlarged view of the 3p, 3d, and 4f orbitals of Eu^{2+} in the crystal were demonstrated. The 5p orbital of iodine and the 3d and 4f orbitals of Eu^{2+} in the crystal were widely distributed. Near the conduction band, the 6p orbital of Pb was distributed and increased. Incorporation of Eu^{2+} ions into the crystal did not influence the pDOS of the 5p orbital of Pb or the 5p orbital of iodine in the crystal. This behaviour suggests a slight influence on the carrier mobility. The electronic behaviour suggests itinerant characteristics, with promotion of the carrier diffusion on the 5p orbital of I in the crystal structure. Incorporation of Eu^{2+} ions into the perovskite crystal provided low energy levels at the VB, with an increase in the bandgap and a decrease in m_h^*/m_e . This behaviour suggests improvement of carrier mobility related to short-circuit current and conversion efficiency, as compared with incorporation of Eu^{3+} ions into the perovskite crystal.

The chemical shifts of ^{127}I -NMR in the $\text{MAPb}(\text{Eu}^{3+})\text{I}_3$ compared to the $\text{MAPb}(\text{Eu}^{2+})\text{I}_3$ crystal were remarkably shifted by nuclear quadrupole interaction in proportion to the extent of the values of Q , EFG tensor, and η . The chemical shifts of ^{127}I -NMR in the $\text{MAPb}(\text{Eu})\text{I}_3$ perovskite crystal depended on the extent of nuclear quadrupole interaction based on the Q -tensor, related to EFG and η of the iodine ligand by the extent of spin-orbital interaction based on electron density distribution and hybridisation of the s, p, and d orbitals of the Eu ion in the coordination structure. The chemical shifts of ^{127}I -NMR in the $\text{MAPb}(\text{Eu}^{3+})\text{I}_3$ perovskite crystal were based on the anisotropic magnetic interaction between the nearest-neighbour ligand and Eu^{3+} ion in the coordination structure. In the case of the $\text{MAPb}(\text{Eu}^{2+})\text{I}_3$ perovskite crystal, the chemical shifts of ^{127}I -NMR suggested isotropic behaviour, with narrow splitting in the magnetic field. The isotropic magnetic interaction was derived from nuclear Zeeman interaction, isotropic hyperfine interaction between electrons and nuclear spins, and nuclear quadrupole interaction based on the EFG and η of the Eu^{2+} ion, with slight extent of electron density distribution on the Eu-I band in the coordination structure.

The electronic correlation based on the charge transfer from the 3d, 4f hybrid orbital of the europium ion to the 5p orbital of the iodine ion as a ligand determined the itinerant system, with increase in the carrier mobility related to the reciprocal of the effective mass of the holes. The anisotropic behaviour was associated with the crystal field perturbation of energy level splitting and the nuclear quadrupole interaction based on EFG and η . The itinerant behaviour promoted an increase in the carrier mobility, predicting improvement of the short-circuit current density. The valence fluctuation of Eu^{2+} and Eu^{3+} ions influenced the charge transfer between metal and ligand in the perovskite crystal. The mechanisms had itinerant variation based on exchange interaction in the coordination structure. The electronic structures of the doping of lanthanide ions into MAPbI_3 perovskite crystals were considered. The electronic correlation with the crystal field perturbation suggests a photovoltaic mechanism, improving the stability of conversion efficiency.

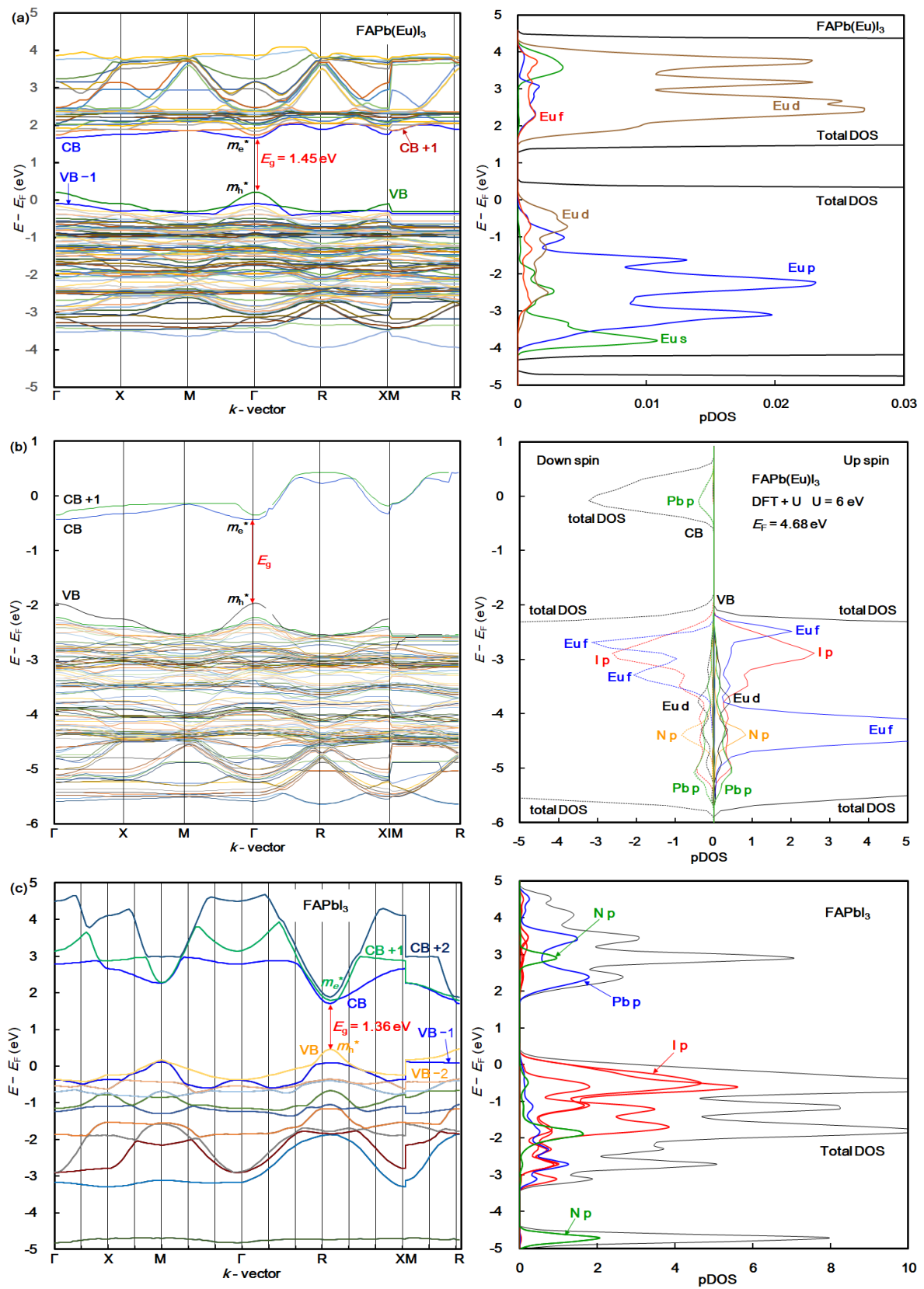


Figure 1. (a) Band structure, (b) density of state, and enlarged view of the 3p, 3d, and 4f orbitals of Eu ion in (a) FAPb(Eu³⁺)I₃, (b) FAPb(Eu²⁺)I₃, and (c) FAPbI₃ crystals. m_e^* and m_h^* : effective mass of electron and hole.

4. Conclusions

Partial replacement of Eu at the Pb site in the perovskite crystal influenced the electronic structure, and the effective mass was related to carrier mobility and E_g via energy level at the VB state. In the case of the FAPb(Eu⁺³)I₃ crystal, the 3d and 4f orbitals of the Eu ion appeared near the VB, and the 3d orbital was widely distributed near the CB. The effective mass ratio was slightly increased by the incorporation of Eu⁺³ ions. In the case of the FAPb(Eu⁺²)I₃ crystal, the 4f orbital of the Eu⁺² ion and the 5p orbital of the iodine ion strongly appeared near the VB, and the 3d orbital of the Eu⁺² ion and the 5p orbital of the Pb ion were distributed near the CB. Incorporation of Eu⁺² ions into the crystal decreased the effective mass ratio, promoting the carrier diffusion related to the mobility, suggesting improvement in the short-circuit current density and conversion efficiency. The chemical shifts of ¹²⁷I-NMR of the MAPb(Eu⁺²)I₃ crystal depended on the extent of the nuclear quadrupole interaction based on EFG and η in the coordination structure. The electronic correlation promoted the charge transfer, improving the short-circuit current density and conversion efficiency.

Author Contributions: Conceptualisation, A.S.; methodology, A.S.; software, A.S.; validation, A.S.; formal analysis, A.S.; investigation, A.S.; resources, A.S.; data curation, A.S.; writing—original draft preparation, A.S.; writing—review and editing, A.S. and T.O.; visualisation, A.S.; supervision, T.O.; project administration, T.O.; funding acquisition, A.S. and T.O. All authors have read and agreed to the published version of the manuscript.

Funding: This research was supported by JSPS KAKENHI Grant Number 21K05261.

Institutional Review Board Statement: Not applicable.

Informed Consent Statement: Not applicable.

Data Availability Statement: All data generated and analyzed during this study are included in this published article.

Conflicts of Interest: The authors declare no conflict of interest.

References

1. Dunfield, S.P.; Bliss, L.; Zhang, F.; Luther, J.M.; Zhu, K.; Hest, M.F.A.M.; Reese, M.O.; Berry, J.J. From defects to degradation: A mechanistic understanding of degradation in perovskite solar cell devices and modules. *Adv. Energy Mater.* **2020**, *10*, 1904054. [[CrossRef](#)]
2. Jeong, M.; Choi, I.W.; Go, E.M.; Cho, Y.; Kim, M.; Lee, B.; Jeong, S.; Jo, Y.; Choi, H.W.; Lee, J.; et al. Stable perovskite solar cells with efficiency exceeding 24.8% and 0.3-V voltage loss. *Science* **2020**, *369*, 1615–1620. [[CrossRef](#)] [[PubMed](#)]
3. Yang, Z.; Yu, Z.; Wei, H.; Xiao, X.; Ni, Z.; Chen, B.; Deng, Y.; Habisreutinger, S.N.; Chen, X.; Wang, K.; et al. Enhancing electron diffusion length in narrow-bandgap perovskites for efficient monolithic perovskite tandem solar cells. *Nat. Commun.* **2019**, *10*, 4498. [[CrossRef](#)] [[PubMed](#)]
4. Li, Z.; Kim, T.H.; Han, S.Y.; Yun, Y.J.; Jeong, S.; Jo, B.; Ok, S.A.; Yim, W.; Lee, S.H.; Kim, K.; et al. Wide-bandgap perovskite/gallium arsenide tandem solar cells. *Adv. Energy Mater.* **2020**, *10*, 1903085. [[CrossRef](#)]
5. Kim, D.; Jung, H.J.; Park, I.J.; Larson, B.W.; Dunfield, S.P.; Xiao, C.; Kim, J.; Tong, J.; Boonmongkolras, P.; Ji, S.G.; et al. Efficient, stable silicon tandem cells enabled by anion-engineered wide-bandgap perovskites. *Science* **2020**, *368*, 155–160. [[CrossRef](#)]
6. McMeekin, D.P.; Sadoughi, G.; Rehman, W.; Eperon, G.E.; Saliba, M.; Hörantner, M.T.; Haghighirad, A.; Sakai, N.; Korte, L.; Rech, B.; et al. A mixed-cation lead mixed-halide perovskite absorber for tandem solar cells. *Science* **2016**, *351*, 151–155. [[CrossRef](#)]
7. Kishimoto, T.; Suzuki, A.; Ueoka, N.; Oku, T. Effects of guanidinium addition to CH₃NH₃PbI_{3-x}Cl_x perovskite photovoltaic devices. *J. Ceram. Soc. Jpn.* **2019**, *127*, 491–497. [[CrossRef](#)]
8. Wang, Y.; Dar, M.I.; Ono, L.K.; Zhang, T.; Kan, M.; Li, Y.; Zhang, L.; Wang, X.; Yang, Y.; Gao, X.; et al. Thermodynamically stabilized β -CsPbI₃-based perovskite solar cells with efficiencies >18%. *Science* **2019**, *365*, 591–595. [[CrossRef](#)]
9. Chen, Y.; Li, N.; Wang, L.; Li, L.; Xu, Z.; Jiao, H.; Liu, P.; Zhu, C.; Zai, H.; Sun, M.; et al. Impacts of alkaline on the defects property and crystallization kinetics in perovskite solar cells. *Nat. Commun.* **2019**, *10*, 1112. [[CrossRef](#)]
10. Oku, T.; Kandori, S.; Taguchi, M.; Suzuki, A.; Okita, M.; Minami, S.; Fukunishi, S.; Tachikawa, T. Polysilane-inserted methylammonium lead iodide perovskite solar cells doped with formamidinium and potassium. *Energies* **2020**, *13*, 4776. [[CrossRef](#)]
11. Jodlowski, A.D.; Carmona, C.R.; Grancini, G.; Salado, M.; Ralaiarisoa, M.; Ahmad, S.; Koch, N.; Camacho, L.; Miguel, G.; Nazeeruddin, M.K. Large guanidinium cation mixed with methylammonium in lead iodide perovskites for 19% efficient solar cells. *Nat. Energy* **2017**, *2*, 972–979. [[CrossRef](#)]

12. Saidaminov, M.I.; Kim, J.; Jain, A.; Bermudez, R.Q.; Tan, H.; Long, G.; Tan, F.; Johnston, A.; Zhao, Y.; Voznyy, O.; et al. Suppression of atomic vacancies via incorporation of isovalent small ions to increase the stability of halide perovskite solar cells in ambient air. *Nat. Energy* **2018**, *3*, 648–654. [[CrossRef](#)]
13. Gong, X.; Guan, L.; Pan, H.; Sun, Q.; Zhao, X.; Li, H.; Pan, H.; Shen, Y.; Shao, Y.; Sun, L.; et al. Highly efficient perovskite solar cells via nickel passivation. *Adv. Funct. Mater.* **2018**, *28*, 1804286. [[CrossRef](#)]
14. Zheng, H.; Liu, G.; Xu, X.; Alsaedi, A.; Hayat, T.; Pan, X.; Dai, S. Acquiring high-performance and stable mixed-dimensional perovskite solar cells by using a transition-metal-substituted Pb precursor. *ChemSusChem* **2018**, *11*, 3269–3275. [[CrossRef](#)] [[PubMed](#)]
15. Suzuki, A.; Oku, T. Effects of transition metals incorporated into perovskite crystals on the electronic structures and magnetic properties by first-principles calculation. *Heliyon* **2018**, *4*, e00755. [[CrossRef](#)]
16. Kooijman, A.; Muscarella, L.A.; Williams, R.M. Perovskite thin film materials stabilized and enhanced by Zinc(II) doping. *Appl. Sci.* **2019**, *9*, 1678. [[CrossRef](#)]
17. Zhu, H.X.; Wang, X.H.; Zhuang, G.C. Electronic structure, magnetism properties and optical absorption of organometal halide perovskite $\text{CH}_3\text{NH}_3\text{XI}_3$ ($X = \text{Fe}, \text{Mn}$). *Appl. Phys. A* **2019**, *125*, 45. [[CrossRef](#)]
18. Ueoka, N.; Oku, T.; Suzuki, A. Additive effects of alkali metals on Cu-modified $\text{CH}_3\text{NH}_3\text{PbI}_{3-\delta}\text{Cl}_\delta$ photovoltaic devices. *RSC Adv.* **2019**, *9*, 24231. [[CrossRef](#)]
19. Suzuki, A.; Kitagawa, K.; Oku, T.; Okita, M.; Fukunishi, S.; Tachikawa, T. Additive effects of copper and alkali metal halides into methylammonium lead iodide perovskite solar cells. *Electron. Mater. Lett.* **2022**, *18*, 176–186. [[CrossRef](#)]
20. Wang, K.L.; Wang, R.; Wang, Z.K.; Li, M.; Zhang, Y.; Ma, H.; Liao, L.S.; Yang, Y. Tailored phase transformation of CsPbI_2Br films by copper(II) bromide for high-performance all-inorganic perovskite solar cells. *Nano Lett.* **2019**, *19*, 5176. [[CrossRef](#)]
21. Ueoka, N.; Oku, T. Effects of co-addition of sodium chloride and copper(II) bromide to mixed-cation mixed-halide perovskite photovoltaic devices. *ACS Appl. Energy Mater.* **2020**, *3*, 7272–7283. [[CrossRef](#)]
22. Tong, J.; Song, Z.; Kim, D.H.; Chen, X.; Chen, C.; Palmstrom, A.F.; Ndione, P.F.; Reese, M.O.; Dunfield, S.P.; Reid, O.G.; et al. Carrier lifetimes of $>1 \mu\text{s}$ in Sn-Pb perovskites enable efficient all-perovskite tandem solar cells. *Science* **2019**, *364*, 475–479. [[CrossRef](#)] [[PubMed](#)]
23. Peng, L.; Xie, W. Theoretical and experimental investigations on the bulk photovoltaic effect in lead-free perovskites MASnI_3 and FASnI_3 . *RSC Adv.* **2020**, *10*, 14679–14688. [[CrossRef](#)] [[PubMed](#)]
24. Suzuki, A.; Kato, M.; Ueoka, N.; Oku, T. Additive effect of formamidinium chloride in methylammonium lead halide compound-based perovskite solar cells. *J. Electron. Mater.* **2019**, *48*, 3900–3907. [[CrossRef](#)]
25. Li, N.; Tao, S.; Chen, Y.; Niu, X.; Onwudinanti, C.K.; Hu, C.; Qiu, Z.; Xu, Z.; Zheng, G.; Wang, L.; et al. Cation and anion immobilization through chemical bonding enhancement with fluorides for stable halide perovskite solar cells. *Nat. Energy* **2019**, *4*, 408–415. [[CrossRef](#)]
26. Xu, W.; Zheng, L.; Zhang, X.; Cao, Y.; Meng, T.; Wu, D.; Liu, L.; Hu, W.; Gong, X. Efficient perovskite solar cells fabricated by Co partially substituted hybrid perovskite. *Adv. Energy Mater.* **2018**, *8*, 1703178. [[CrossRef](#)]
27. Suzuki, A.; Oku, T. First-principles calculation study of electronic structures of alkali metals (Li, K, Na and Rb)-incorporated formamidinium lead halide perovskite compounds. *Appl. Surf. Sci.* **2019**, *483*, 912–921. [[CrossRef](#)]
28. Suzuki, A.; Miyamoto, Y.; Oku, T. Electronic structures, spectroscopic properties, and thermodynamic characterization of sodium- or potassium-incorporated $\text{CH}_3\text{NH}_3\text{PbI}_3$ by first-principles calculation. *J. Mater. Sci.* **2020**, *55*, 9728–9738. [[CrossRef](#)]
29. Oku, T. Crystal structures of perovskite halide compounds used for solar cells. *Rev. Adv. Mater. Sci.* **2020**, *59*, 264–305. [[CrossRef](#)]
30. Suzuki, A.; Oku, T. Electronic structures and magnetic properties of transition metal doped CsPbI_3 perovskite compounds by first-principles calculation. *Phys. Solid State* **2019**, *61*, 1074–1085. [[CrossRef](#)]
31. Suzuki, A.; Oe, M.; Oku, T. Fabrication and characterization of Ni-, Co-, and Rb-incorporated $\text{CH}_3\text{NH}_3\text{PbI}_3$ perovskite solar cells. *J. Electron. Mater.* **2021**, *50*, 1980–1995. [[CrossRef](#)]
32. Pazoki, M.; Edvinsson, T. Metal replacement in perovskite solar cell materials: Chemical bonding effects and optoelectronic properties. *Sustain. Energy Fuels* **2018**, *2*, 1430–1445. [[CrossRef](#)]
33. Wang, L.; Zhou, H.; Hu, J.; Huang, B.; Sun, M.; Dong, B.; Zheng, G.; Huang, Y.; Chen, Y.; Li, L.; et al. A Eu^{3+} - Eu^{2+} ion redox shuttle imparts operational durability to Pb-I perovskite solar cells. *Science* **2019**, *363*, 265–270. [[CrossRef](#)] [[PubMed](#)]
34. Bala, A.; Kumar, V. Stability of the Eu^{2+} dopant in CsPbBr_3 perovskites: A first-principles study. *J. Phys. Chem. C* **2019**, *123*, 6965–6969. [[CrossRef](#)]
35. Tian, J.; Xue, Q.; Yao, Q.; Li, N.; Brabec, C.J.; Yip, H.L. Inorganic halide perovskite solar cells: Progress and challenges. *Adv. Energy Mater.* **2020**, *10*, 2000183. [[CrossRef](#)]
36. Chen, Y.; Liu, S.; Zhou, N.; Li, N.; Zhou, H.; Sun, L.D.; Yan, C.H. An overview of rare earth coupled lead halide perovskite and its application in photovoltaics and light emitting devices. *Prog. Mater. Sci.* **2020**, *18*, 100737. [[CrossRef](#)]
37. Yang, S.; Zhao, H.; Han, Y.; Duan, C.; Liu, Z.; Liu, S.F. Europium and acetate Co-doping strategy for developing stable and efficient CsPbI_2Br perovskite solar cells. *Small* **2019**, *15*, 1904387. [[CrossRef](#)]
38. Song, Z.; Xu, W.; Wu, Y.; Liu, S.; Bi, W.; Chen, X.; Song, H. Incorporating of lanthanides ions into perovskite film for efficient and stable perovskite solar cells. *Small* **2020**, *16*, 2001770. [[CrossRef](#)]
39. Pazoki, M.; Röckert, A.; Wolf, M.J.; Imani, R.; Edvinsson, T.; Kullgren, J. Electronic structure of organic–inorganic lanthanide iodide perovskite solar cell materials. *J. Mater. Chem. A* **2017**, *5*, 23131–23138. [[CrossRef](#)]

40. Suzuki, A.; Oku, T. Effects of mixed-valence states of Eu-doped FAPbI₃ perovskite crystals studied by first-principles calculation. *Mater. Adv.* **2021**, *2*, 2609–2616. [[CrossRef](#)]
41. Weller, M.T.; Weber, O.J.; Frost, J.M.; Walsh, A. Cubic perovskite structure of black formamidinium lead iodide, α -[HC(NH₂)₂]PbI₃, at 298 K. *J. Phys. Chem. Lett.* **2015**, *6*, 3209–3212. [[CrossRef](#)]
42. Mashiyama, H.; Kurihara, Y.; Azetsu, T. Disordered cubic perovskite structure of CH₃NH₃PbX₃ (X = Cl, Br, I). *J. Korean Phys. Soc.* **1998**, *32*, S156–S158.